Histochemical examination of blood vessels in murine femora with intermittent PTH administration

Haruhi Maruoka[a*], Shen Zhao[c*], Hirona Yoshino[a], Miki Abe[a], Tomomaya Yamamoto[a, d], Hiromi Hongo[a], Mai Haraguchi-Kitakamae[a, e], Alireza Nasoori[a], Hotaka Ishizu[a,b], Yuhi Nakajima[a], Masayuki Omaki[a], Tomohiro Shimizu[b], Norimasa Iwasaki[b], Paulo Henrique Luiz de Freitas[f], Minqi Li[g] and Tomoka Hasegawa[a#]

[a]Developmental Biology of Hard Tissue, Faculty of Dental Medicine, [b]Orthopedic Surgery, Faculty of Medicine, Hokkaido University, Sapporo, Japan, [c]Department of Endodontics and Operative Dentistry, Shanghai Ninth People's Hospital, College of Stomatology, Shanghai Jiao Tong University School of Medicine, Shanghai, China, [d]Northern Army Medical Unit, Camp Makomanai, Japan Ground Self-Defense Forces, Sapporo, Japan, [e]Division of Craniofacial Development and Tissue Biology, Graduate School of Dentistry, Tohoku University, Sendai, Japan, [f]Department of Dentistry, Federal University of Sergipe, Lagarto, SE, Brazil, [g]Shandong Provincial Key Laboratory of Oral Biomedicine, The School of Stomatology, Shandong University, Jinan, China

*These authors equally contributed to this work.

Abbreviated Title: ***Perivascular stromal cells after PTH administration***

[#]Address for correspondence:

Tomoka Hasegawa, DDS, PhD
Developmental Biology of Hard Tissue
Graduate School of Dental Medicine, Hokkaido University
Kita 13 Nishi 7 Kita-ku
Sapporo 060-8586, Japan
Tel/Fax: +81-11-706-4226
E-mail: hasegawa@den.hokudai.ac.jp

Abstract

Objective: To verify the biological effects of parathyroid hormone (PTH) on the blood vessels in the bone, this study aimed to investigate histological alterations in endomucin-positive blood vessels and perivascular cells in murine femora after intermittent PTH administration. For comparison with blood vessels in the bone, we examined the distribution of endomucin-positive blood vessels and surrounding αSMA-immunoreactive perivascular cells in the liver, kidney, and aorta with or without PTH administration.

Methods: Six-week-old male C57BL/6J mice received hPTH [1-34] or vehicle for two weeks. All mice were fixed with a paraformaldehyde solution after euthanasia, and the right femora, kidney, liver, and aorta were extracted for immunohistochemical analysis of endomucin, αSMA, ephrinB2, EphB4, and HIF1α. Light microscopic observations of semi-thin sections and transmission electron microscopic (TEM) observations of ultra-thin sections were performed on the left femora.

Results: After intermittent PTH administration, αSMA-reactive/ephrinB2-positive stromal cells appeared around endomucin-positive/EphB4-immunoreactive blood vessels in the bone. In addition, intense immunoreactivities of EphB4 and HIF1α were seen in vascular endothelial cells after the PTH treatment. Several stromal cells surrounding PTH-treated blood vessels exhibited well-developed rough endoplasmic reticulum under TEM observations. In contrast to bone tissues, αSMA-positive stromal cells did not increase around the endomucin-positive blood vessels in the kidney, liver, or aorta, even after PTH administration.

Conclusion: These findings show that intermittent PTH administration increases αSMA-reactive/ephrinB2-positive perivascular stromal cells in bone tissue but not in the kidney, liver, or aorta, suggesting that PTH preferentially affects blood vessels in the bone.

Keywords: *blood vessels, perivascular stromal cells, parathyroid hormone (PTH), endomucin, αSMA*

1 Introduction

Parathyroid hormone (PTH) is currently used for the treatment of osteoporosis due to its bone mass-increasing properties [1-3]. Previous studies have reported that intermittent PTH administration increases bone mass by promoting osteoblastic bone formation as well as inducing preosteoblastic proliferation [4,5]. On the other hand, several reports have suggested biological effects of PTH on the blood vessels in bone [6-8]. For example, PTH [1-34] treatment increased the number of blood vessels at the fracture site and stabilized it early in a femur fracture mice model [7]. Furthermore, we have demonstrated that intermittent administration of PTH increased the number and diameter of endomucin-positive bone-specific vessels as well as that of αSMA(+)/TNALP(+)/c-kit(+) perivascular stromal cells around the blood vessels in mice [8].

Kusumbe *et al.* [9] and Rammsay *et al.* [10] have recently divided blood vessels in bone into type H and type L vessels. The blood vessels of type H show intense CD31-reactivity and endomucin-positivity, whereas those of type L yield weak CD31-reactivity/endomucin-positivity in murine long bones. Endomucin is a mucin-like sialoglycoprotein with a molecular weight of 80–120 kDa that is only expressed on the vascular endothelial cells of capillary and venous [11-14]. Kusumbe *et al.* [9] have demonstrated that strongly endomucin-positive blood vessels interact with osteoblasts in bone tissue. In addition, the authors verified that hypoxia-inducible factor (HIF1) α increased the number of endomucin-positive blood vessels and of Runx2-positive/osterix-positive osteoblasts in bone [9]. It has also been reported that the miR-497-195 cluster, which is highly expressed in endomucin-positive blood vessels, maintains Notch activity and HIF1α stability in vascular endothelial cells in bone [15]. These findings suggest that HIF1α may promote both angiogenesis and osteoblastic bone formation via the induction of endomucin-positive blood vessels.

EphB4 and ephrinB2 are involved in the regulation of angiogenesis, with EphB4, a receptor for ephrinB2, expressed in the vascular endothelial cells of veins and ephrinB2 in the vascular endothelial cells of arteries and arterioles [16]. In our previous study, endomucin-positive blood vessels showed EphB4 immunoreactivity in the femoral metaphyses of murine bone [17]. EphB4/ephrinB2 signaling is also known as a coupling factor between osteoblasts and osteoclasts, which suggests that endomucin-positive/EphB4-positive blood vessels may affect

the bone cells via ephrinB2 signaling (Zhao *et al.,* 2006; Allan *et al.,* 2008; Martin *et al.,* 2010; Chen *et al.,* 2018; Baek *et al.,* 2018). αSMA-positive perivascular stromal cells, which have been found to increase around blood vessels after intermittent PTH administration, show TNALP and c-kit positivity (Zhao *et al.,* 2021). Thus, these cells have the potential to differentiate into osteoblast lineage cells via EphB4/ephrinB2 signaling.

Taken together, in this study, we examined the localization of EphB4, ephrinB2, and HIF1α in endomucin-positive blood vessels and αSMA-immunoreactive perivascular stromal cells after intermittent PTH administration. In addition, since endomucin-positive blood vessels have been found not only in bone but also in various tissues throughout the body, including the liver, kidney, and lung, we also investigated the localization of endomucin-positive blood vessels and αSMA-immunoreactive perivascular–stromal cells in the liver, kidney, and aorta after the administration of PTH.

2 Materials and methods

2.1 Animals

Six-week-old male C57BL/6J mice (n=12, Japan CLEA, Tokyo, Japan) were divided into a control group receiving vehicle only (0.9% saline; n=6) and a PTH group receiving hPTH [1-34] (Sigma-Aldrich Co., LLC., St. Louis, MO; n=6). The mice received 20 μg/kg/day of hPTH [1-34] every 12 h for 2 weeks, as previously described (Yamamoto *et al.,* 2016). The experimental protocol was approved by the Hokkaido University Animal Care and Use Committee, which is accredited by the Association for Assessment and Accreditation of Laboratory Animal Care (AAALAC) International (approval no. 20-0019).

2.2 Specimen preparation

All mice were euthanized with an intraperitoneal injection of a combination of anesthetic agents, prepared with 0.3 mg/kg of medetomidine, 4.0 mg/kg of midazolam, and 5.0 mg/kg of butorphanol. Subsequently, they were perfused with 4% paraformaldehyde solution diluted in 0.067 M phosphate buffer (pH 7.4) through the left cardiac ventricle 6 h after receiving the last vehicle or hPTH [1-34], as previously reported (Yamamoto *et al.,* 2016). The femora, kidney,

liver, and aorta were extracted from the mice, and then immersed in 4% paraformaldehyde solution diluted in a 0.067 M phosphate buffer (pH 7.4) for 24 h at 4 °C. After fixation, the femora were decalcified for 1 month with 10% ethylenediamine tetraacetic disodium salt (EDTA-2Na) for light microscopic observations or 5% EDTA-2Na for transmission electron microscopic (TEM) observations and then embedded in paraffin or epoxy resin. For paraffin embedding, the decalcified right femora, kidney, liver, and aorta were dehydrated in ascending ethanol solutions. All the paraffin sections subjected to the following immunohistochemistry were photographed under a Nikon Eclipse Ni microscope (Nikon Instruments Inc. Tokyo, Japan). Light microscopic images were acquired with a digital camera (Nikon DXM1200C, Nikon). For epoxy resin embedding, the decalcified left femora were post-fixed with 1% osmium tetraoxide in a 0.1 M cacodylate buffer for 4 h at 4 °C, dehydrated in ascending acetone solutions, and embedded in epoxy resin (Epon 812; Taab, Berkshire, UK).

2.3 Single immunohistochemical staining

For immunodetection using horseradish peroxidase (HRP)-conjugated secondary antibodies, all dewaxed paraffin sections were subjected to endogenous peroxidase activity inhibition by soaking in methanol containing 0.3% hydrogen peroxidase for 30 min and pretreatment with 1% bovine serum albumin (BSA; Serologicals Proteins, Inc., Kankakee, IL) in PBS (1% BSA-PBS) for 30 min. After that, sections were incubated with the corresponding pair of antibodies according to the antigen of interest (primary/secondary), as follows: 1) EphB4, goat antibody against mouse EphB4 (#AF446, R&D Systems, Inc., Minneapolis, MN; diluted 1: 50)/HRP-conjugated anti-goat IgG (#A201PS, American Qualex Scientific Products, Inc., San Clemente, CA; diluted 1: 100); 2) HIF1α, rabbit polyclonal anti-HIF1a (#GTX127309, Gene Tex, Inc., Irvine, CA; diluted 1: 100)/HRP-conjugated anti-rabbit IgG (#P0399, DakoCytomation, Glostrup, Denmark; diluted 1: 100); 3) endomucin, rat antibody against endomucin (#sc-65495, Santa Cruz Biotechnology, Inc., Dallas, TX; diluted 1:100)/HRP-conjugated anti-rat IgG (#A18921, Zymed Laboratories Inc., South San Francisco, CA; diluted 1: 100); 4) αSMA, mouse antibody against αSMA (#AF446, R&D Systems; diluted 1: 400)/HRP-conjugated anti-mouse IgG (#61-6520, Chemicon International Inc., Temecula, CA; diluted 1: 100). Immunoreactions were assessed using 3, 3'-diaminobenzidine tetrahydrochloride (Dojindo Laboratories, Kumamoto, Japan).

2.4 Double immunofluorescent staining

For the endomucin/αSMA double immunohistochemical staining, dewaxed paraffin sections were incubated with 1% BSA-PBS, then with anti-endomucin antibody (Santa Cruz), and subsequently with Alexa 594-conjugated anti-rat IgG (#A-21211, Invitrogen Co., Camarillo, CA). The sections were subsequently incubated with mouse antibody against αSMA (R&D Systems) and reacted with Alexa 488-conjugated anti-mouse IgG (#A-11001, Invitrogen Co.), diluted 1: 100. For the detection of endomucin/ephrinB2 and αSMA/ephrinB2, dewaxed paraffin sections were reacted with endomucin antibody (Santa Cruz), or with αSMA antibody (R&D Systems), and then labeled with Alexa 594-conjugated anti-rat IgG or Alexa 594-conjugated anti-mouse IgG (#A-21203, Invitrogen Co.). The immuno-labeled sections were reacted with goat antibody against ephrinB2 (#AF496, R&D Systems; diluted 1: 50), and then incubated with Alexa 488-conjugated anti-goat IgG (#A-11055, Invitrogen Co.; diluted 1: 100). The sections were embedded using VECTASHIELD hard-set mounting medium with DAPI (Vector Laboratories, Inc. Burlingame, CA) and observed using a fluorescence microscope.

2.5 Transmission electron microscopic observation

Histological sections of epoxy resin-embedded decalcified specimens were prepared with an ultramicrotome (Sorvall MT-5000; Ivan Sorvall, Inc., Norwalk, CT), stained with toluidine blue and observed under a light microscope. Ultra-thin sections were cut with an ultramicrotome and stained with uranyl acetate and lead citrate for TEM observation (Hitachi H-7100; Hitachi Co. Ltd, Tokyo, Japan) at 80 kV.

3 Results

In the control femur, most blood vessels exhibited immunoreactivity for endomucin; however, only very few αSMA-positive blood vessels were observed (**Fig. 1A**). In contrast, αSMA-positive blood vessels were detected after the intermittent PTH administration (**Fig. 1D**). αSMA-positive stromal cells spread out of the endomucin-positive blood vessels (**Fig. 1D**). The double detection of endomucin/ephrinB2 showed that endomucin-positive blood vessels were

distant from ephrinB2-reactive osteoblasts in the control mice (**Fig. 1B**). In the PTH-treated mice, however, ephrinB2-positivity was observed not only in the osteoblastic layer but also in the vicinity of the endomucin-positive blood vessels (**Fig. 1E**). As shown in **Fig. 1F**, the thick layer of αSMA-reactive perivascular cells either overlapped with ephrinB2 reactivity or was located in close proximity to ephrinB2-reactive osteoblasts in PTH-treated mice.

Since ephrinB2 could interact with EphB4 [18-22], we examined the localization of EphB4. Although EphB4 immunoreactivity was localized on the vascular endothelial cells in both the control and PTH-treated specimens, it was more evident in the PTH-treated specimens (**Fig. 2A** and **B**). Semi-thin sections showed numerous preosteoblasts and various types of stromal cells between the blood vessels and osteoblasts in the PTH-treated mice (**Fig. 2D**), whereas lower numbers of preosteoblasts were found in the corresponding region in the control mice (**Fig. 2C**).

The intensity of HIF1α, which induces transcription of angiogenesis-related genes such as VEGF in response to hypoxia [23-25], increased in reaction to the intermittent PTH administration. Although both the control and PTH-treated specimens displayed HIF1α immunoreactivity in blood vessels, it seemed more evident after PTH administration (compare **Fig. 3A** and **B**). TEM observation showed increased cell density in the region between the blood vessels and osteoblasts after PTH administration compared to the control (**Fig. 4A** and **B**). A variety of stromal cells occupied the region between the blood vessels and osteoblasts in the PTH-treated femora (**Fig. 4C**), but when observed at a higher magnification, these stromal cells possessed abundant rough endoplasmic reticulum and Golgi apparatus, indicating the potential to synthesize extracellular matrices (**Fig. 4D**).

Finally, we examined the distribution of endomucin-positive blood vessels and αSMA-immunoreactive perivascular cells in the kidney, liver, and aorta of control and PTH-treated mice. In both groups of mice, endomucin immunopositivity was detectable in the vascular endothelial cells of glomeruli and peritubular capillaries of the kidney (**Fig. 5A, C**), the central veins and sinusoidal capillaries of the liver (**Fig. 5E, G**), and the tunica intima of the aorta (**Fig. 5I, K**). Unlike the blood vessels in bone tissue, numbers of αSMA-positive cells did not increase in association with the endomucin-reactive blood vessels of the kidney (**Fig. 5D**), the sinusoid of the liver **(Fig 5H),** and the tunica media of the aorta **(Fig. 5L**) in PTH-treated mice compared to the respective control specimens (**Fig. 5B, F, J**).

4 Discussion

In this study, we found that intermittent PTH administration leads to an increase in αSMA(+)/ephrinB2(+) stromal cells around endomucin-positive and EphB4-reactive blood vessels in bone tissue, whereas such cells did not appear in other organs. Our previous studies showed that PTH induces Runx2-positive/TNALP-reactive preosteoblasts and αSMA(+)/TNALP(+)/c-kit(+) stromal cells surrounding blood vessels in bone [4,8]. Since we found that most blood vessels express both endomucin and EphB4 in the femoral metaphysis, αSMA-positive/ephrinB2-positive perivascular stromal cells might be committed to the osteogenic lineage via interaction with EphB4-positive vascular endothelial cells.

HIF1α promotes the transcription of various proteins such as VEGF, erythropoietin, and glucose transporters to adapt to hypoxic conditions [23-25]. The role of HIF1α is thought to be closely related to the regulation of angiogenesis-osteogenesis coupling [26-30]. The report by Kusumbe et al. [9] indicated that HIF1α increases the number of endomucin-positive blood vessels and Runx2-positive/osterix-positive osteoblasts, which suggests the promotion of bone formation. Similarly, there are reports that PTH treatment increases the expression levels of HIF1α protein in primary mice osteoblasts [31], and that PTH decreases the gene expression of *Hif1α* in cultured osteoblastic UMR106.01 cells [32]. These reports provide conflicting results and the discrepancy has not been settled yet. Our current study shows HIF1α immunoreactivity in bone tissue on the vascular endothelial cells, perivascular cells, and osteoblasts after intermittent PTH administration. Taken together, our findings suggest that PTH contributes to the increase in αSMA-reactive perivascular stromal cells via increased HIF1α expression in bone.

Endomucin-positive blood vessels were found extensively in the liver and kidney as well as in bone in both control and PTH-treated mice. However, αSMA-positive stromal cells around endomucin-positive blood vessels were observed only in bone tissue after intermittent PTH administration. Although PTH receptors are expressed on vascular endothelial cells of bone as well as on renal vascular endothelial cells [33], we detected no αSMA-positive perivascular stromal cells around endomucin-positive vessels in the kidney and liver. These findings suggest that PTH preferentially affects blood vessels in bone but not in the kidney, liver, or aorta.

5 Conclusion

Our study strongly suggests the possibility that intermittent PTH administration would increase in the number of αSMA-reactive/ephrinB2-positive perivascular stromal cells in bone, but not in kidneys, livers, and aortae. Therefore, PTH appears to preferentially affects blood vessels in bone tissue when compared with other organs including kidneys, livers, and aortae.

Ethical standards

All animal experiments in this study were conducted following the Hokkaido University Guidelines for Animal Experimentation (approved research proposal no. #20-0019).

Competing interests

The authors declare no competing interests.

Contributors

Hasegawa T designed the study and prepared the first draft of the paper as a corresponding author. Maruoka H and Zhao S are the researchers mainly in charge of this work, including the immunohistochemistry staining and the TEM observation experiments. Hirona Y, Abe M, Yamamoto T, Hongo H, Haraguchi-Kitakamae M, Nasoori A, Ishizu H, Nakajima Y, Oomaki M, and Shimizu T contributed to the experimental work, including the preparation of paraffin samples of PTH-treated mice. Iwasaki N, Freitas PHL, and Li M participated in the discussion of the results and the editing and formatting of the manuscript. All authors revised the paper for intellectual content and approved its final version.

Funding

This study was partially supported by grants from the Japanese Society for the Promotion of Science (JSPS, 19K10040 to Hasegawa T) and partially supported by Kazato Research Foundation (Hasegawa T) and a grant-in-aid for young scientists provided by the Uehara

Memorial Foundation (Hasegawa T).

References

1. Orwoll E, Scheele W, Paul S, Adami S, Syversen U, Diez-Perez A, Kaufman JM, Clancy AD, Gaich GA. The effect of teriparatide [human parathyroid hormone (1–34)] therapy on bone density in men with osteoporosis. J Bone Miner Res 2003; 18: 9–17.
2. Cosman F, Hattersley G, Hu MY, Williams GC, Fitzpatrick LA, Black DM. Effects of abaloparatide-SC on fractures and bone mineral density in subgroups of postmenopausal women with osteoporosis and varying baseline risk factors. J Bone Miner Res 2017; 32: 17–23.
3. Schweser KM, Crist BD. Osteoporosis: a discussion on the past 5 years. Curr Rev Musculoskelet Med 2017; 10: 265–274.
4. Luiz de Freitas PH, Li M, Ninomiya T, Nakamura M, Ubaidus S, Oda K, Udagawa N, Maeda T, Takagi R, Amizuka N. Intermittent PTH administration stimulates pre-osteoblastic proliferation without leading to enhanced bone formation in osteoclast-less c-fos(-/-) mice. J Bone Miner Res 2009; 24: 1586–1597.
5. Yamamoto T, Hasegawa T, Sasaki M, Hongo H, Tsuboi K, Shimizu T, Ohta M, Haraguchi M, Takahata T, Oda K, Freitas PHL, Takakura A, Takao-Kawabata R, Isogai Y, Amizuka N. Frequency of teriparatide administration affects the histological pattern of bone formation in young adult male mice. Endocrinology 2016; 157: 2604–2620.
6. Dhillon RS, Xie C, Tyler W, Calvi LM, Awad HA, Zuscik MJ, O'Keefe RJ, Schwarz EM. PTH-enhanced structural allograft healing is associated with decreased angiopoietin-2-mediated arteriogenesis, mast cell accumulation, and fibrosis. J Bone Miner Res. 2013; 28: 586-597.
7. Jiang X, Xu C, Shi H, Cheng Q. PTH 1-34 improves bone healing by promoting angiogenesis and facilitating MSCs migration and differentiation in a stabilized fracture mouse model. PloS One 2019; 14: e0226163.
8. Zhao S, Hasegawa T, Hongo H, Yamamoto T, Abe M, Yoshida T, Haraguchi M, Freitas PHL, Li M, Tei K, Amizuka N. Intermittent PTH administration increases bone-specific blood vessels and surrounding stromal cells in murine long bones. Calcif Tissue Int. 2021; 108: 391–406.

9. Kusumbe AP, Ramasamy SK, Adams RH. Coupling of angiogenesis and osteogenesis by a specific vessel subtype in bone. Nature 2014; 507: 323–328.
10. Ramasamy SK, Kusumbe AP, Wang L, Adams RH. Endothelial Notch activity promotes angiogenesis and osteogenesis in bone. Nature 2014; 507: 376–380.
11. Morgan SM, Samulowitz U, Darley L, Simmons DL and Vestweber D. Biochemical characterization and molecular cloning of a novel endothelial-specific sialomucin. Blood. 1999; 93: 165–175.
12. Samulowitz U, Kuhn A, Brachtendorf G, Nawroth R, Braun A, Bankfalvi A, Böcker W, Vestweber D. Human endomucin: distribution pattern, expression on high endothelial venules, and decoration with the MECA-79 epitope. Am J Pathol. 2002; 160: 1669–1681.
13. dela Paz NG and D'Amore PA. Arterial versus venous endothelial cells. Cell Tissue Res. 2009; 335: 5–16.
14. Zuercher J, Fritzsche M, Feil S, Mohn L, Berger W. Norrin stimulates cell proliferation in the superficial retinal vascular plexus and is pivotal for the recruitment of mural cells. Hum Mol Genet. 2012; 21: 2619–2630.
15. Yang M, Li CJ, Sun X, Guo Q, Xiao Y, Su T, Tu ML, Peng H, Lu Q, Liu Q, He HB, Jiang TJ, Lei MX, Wan M, Cao X, Luo XH. MiR-497195 cluster regulates angiogenesis during coupling with osteogenesis by maintaining endothelial Notch and HIF-1alpha activity. Nat Commun. 2017; 8: 16003.
16. Wang HU, Chen ZF, and Anderson DJ. Molecular distinction and angiogenic interaction between embryonic arteries and veins revealed by ephrin-B2 and its receptor Eph-B4. Cell. 1998; 93: 741–753.
17. Tsuchiya E, Hasegawa T, Hongo H, Yamamoto T, Abe M, Yoshida T, Zhao S, Tsuboi K, Udagawa N, Henrique Luiz de Freitas P, Li M, Kitagawa Y, Amizuka N. Histochemical assessment on the cellular interplay of vascular endothelial cells and septoclasts during endochondral ossification in mice. Microscopy (Oxf) 2021; 70: 201–214.
18. Zhao C, Irie N, Takada Y, Shimoda K, Miyamoto T, Nishiwaki T, Suda T, Matsuo K. Bidirectional ephrinB2-EphB4 signaling controls bone homeostasis. Cell Metab. 2006; 4: 111–121.
19. Allan EH, H¨ausler KD, Wei T, Gooi JH, Quinn JMW, Crimeen-Irwin B, Pompolo S, Sims NA, Gillespie MT, Onyia JE, Martin TJ. EphrinB2 regulation by PTH and PTHrP revealed by molecular profiling in differentiating osteoblasts. J Bone Miner Res 2008; 23: 1170–1181.

20. Martin T , Allan EH, Ho PW, Gooi JH, Quinn JM, Gillespie MT, Krasnoperov V, Sims NA. Communication between ephrinB2 and EphB4 within the osteoblast lineage. Adv Exp Med Biol. 2010; 658: 51–60.
21. Chen X, Wang Z, Duan N, Zhu G, Schwarz E M, Xie C. Osteoblast-osteoclast interactions. Connect. Tissue Res. 2018; 59: 99–107.
22. Baek JM, Cheon Y-H, Kwak SC, Jun HY, Yoon K-H, Lee MS, Kim JY. Claudin 11 regulates bone homeostasis via bidirectional EphB4-EphrinB2signaling. Exp Mol Med. 2018; 50: 50.
23. Semenza GL. Hypoxia-inducible factor 1: master regulator of O2 homeostasis. Curr Opin Genet Dev. 1998; 8: 588–594.
24. Hirai K, Furusho H, Hirota K, Sasaki H. Activation of hypoxia-inducible factor 1 attenuates periapical inflammation and bone loss. Int J Oral Sci. 2018; 10: 12.
25. Pelster, B, Egg M. Hypoxia-inducible transcription factors in fish: expression, function and interconnection with the circadian clock. J. Exp. Biol. 2018; 221(Pt 13):jeb163709.
26. Riddle RC, Khatri R, Schipani E, Clemens TL. Role of hypoxia-inducible factor-1alpha in angiogenic–osteogenic coupling. J Mol Med (Berl.) 2009; 87: 583–590.
27. Schipani E, Maes C, Carmeliet G, Semenza GL. Regulation of osteogenesis–angiogenesis coupling by HIFs and VEGF. J Bone Miner Res. 2009; 24: 1347–1353.
28. Wan C, Shao J, Gilbert SR, Riddle RC, Long F, Johnson RS, Schipani E, Clemens TL. Role of HIF-1α in skeletal development. Ann NY Acad Sci. 2010; 1192: 322–326.
29. Zhao Q, Shen X, Zhang W, Zhu G, Qi J, Deng L. Mice with increased angiogenesis and osteogenesis due to conditional activation of HIF pathway in osteoblasts are protected from ovariectomy induced bone loss. Bone. 2012; 50: 763–770.
30. Drager J, Harvey EJ, Barralet J. Hypoxia signalling manipulation for bone regeneration. Expert Rev Mol Med. 2015; 17: e6.
31. Frey JL, Stonko DP, Faugere MC, Riddle RC. Hypoxia-inducible factor-1alpha restricts the anabolic actions of parathyroid hormone. Bone Res. 2014; 2: 14005.
32. Wong A, Loots GG, Yellowley CE, Dosé AC, Genetos DC. Parathyroid hormone regulation of hypoxia-inducible factor signaling in osteoblastic cells. Bone. 2015; 81: 97-103.
33. Amizuka N, Lee HS, Kwan MY, Arazani A, Warshawsky H, Hendy GN, Ozawa H, White JH, Goltzman D. Cell-specific expression of the parathyroid hormone (PTH)/PTH-related peptide receptor gene in kidney from kidney-specific and ubiquitous promoters. Endocrinology 1997; 138: 469–481.

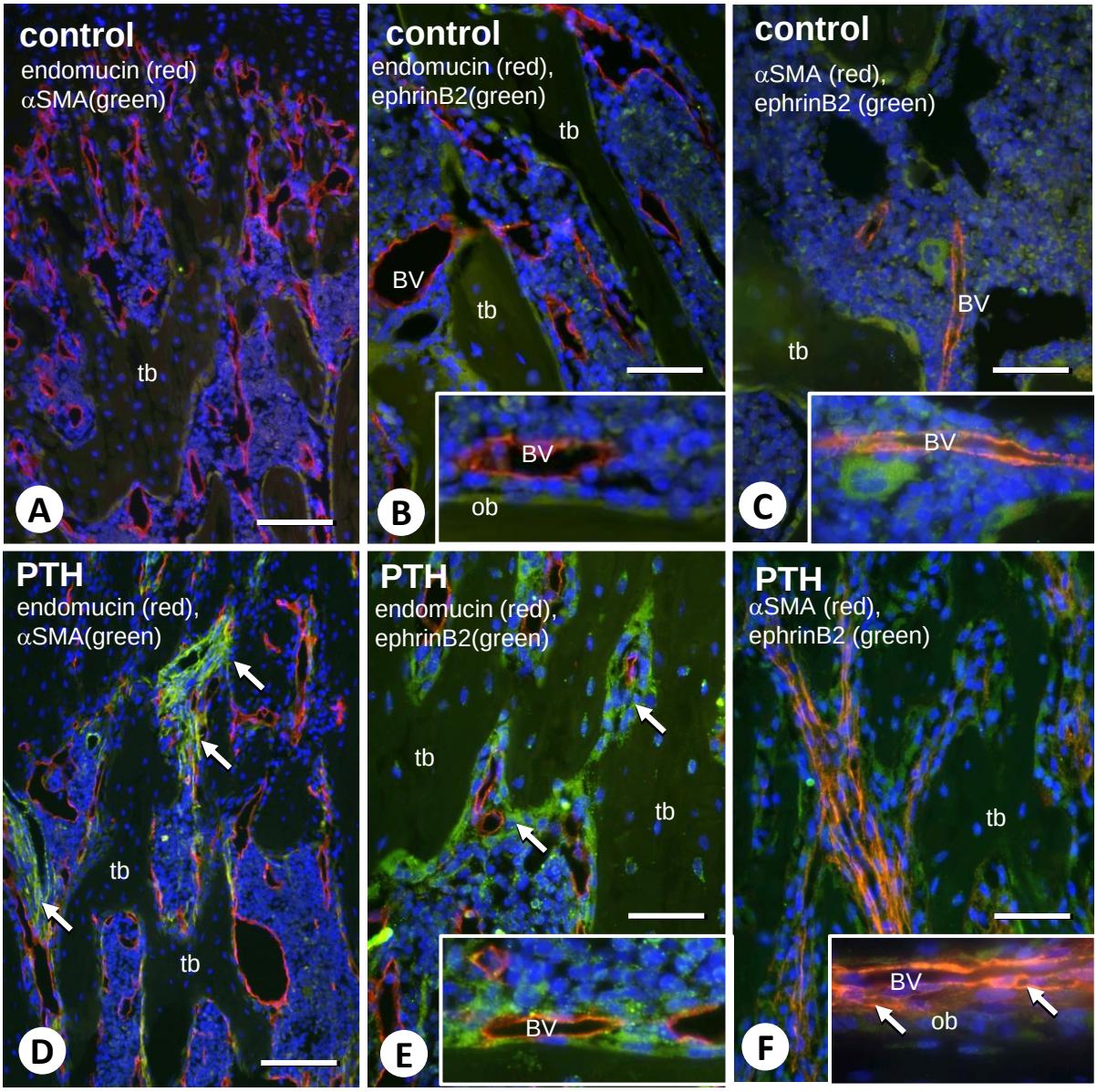
control
endomucin (red)
αSMA(green)
tb
A
control
endomucin (red),
ephrinB2(green)
tb
BV
tb
BV
ob
B
control
αSMA (red),
ephrinB2 (green)
BV
tb
BV
C
PTH
endomucin (red),
αSMA(green)
tb
tb
D
PTH
endomucin (red),
ephrinB2(green)
tb
tb
BV
E
PTH
αSMA (red),
ephrinB2 (green)
tb
BV
ob
F

Fig.1

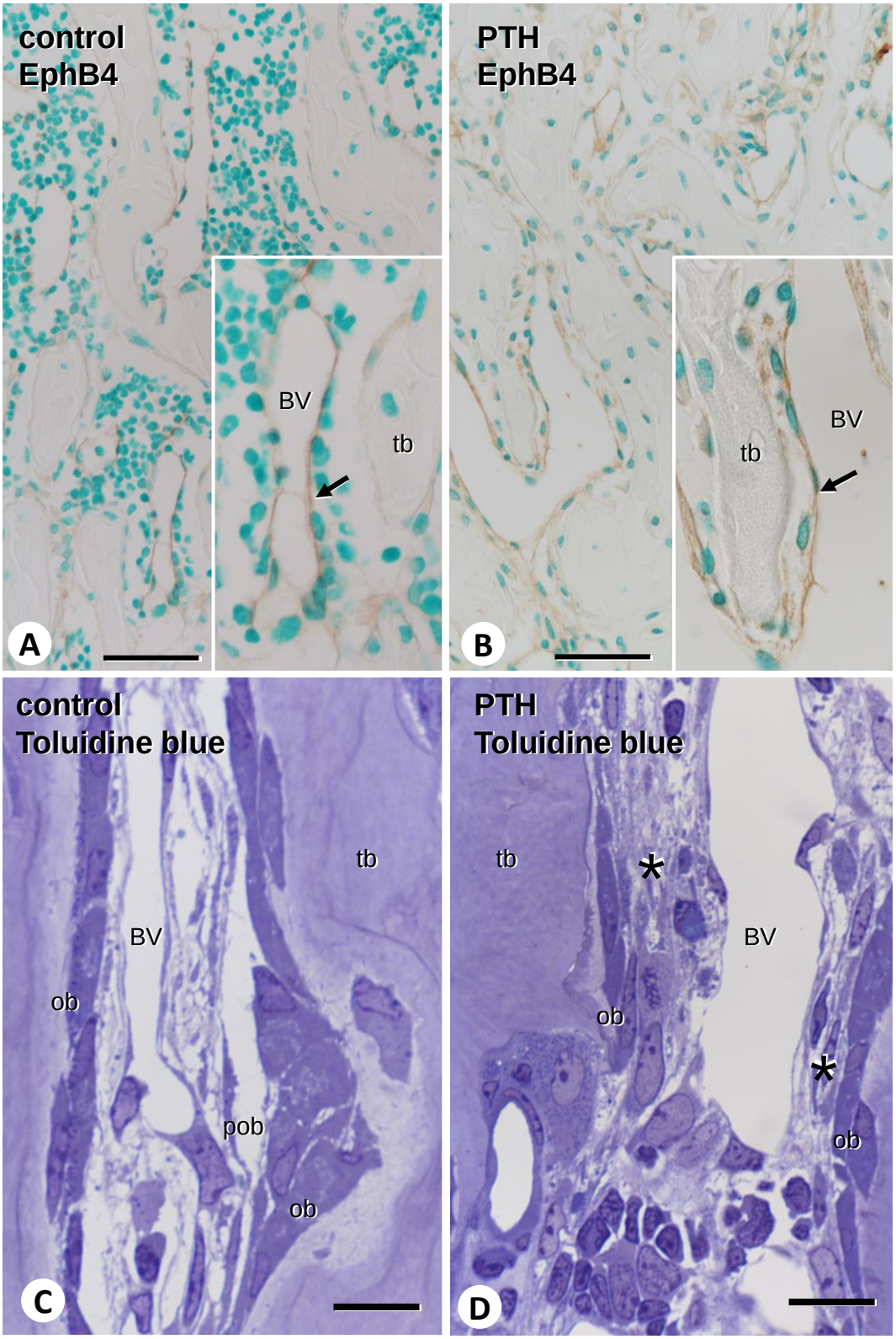
control
EphB4
BV
tb
A
PTH
EphB4
BV
tb
B
control
Toluidine blue
tb
BV
ob
pob
ob
C
PTH
Toluidine blue
tb
*
BV
ob
*
ob
D

Fig.2

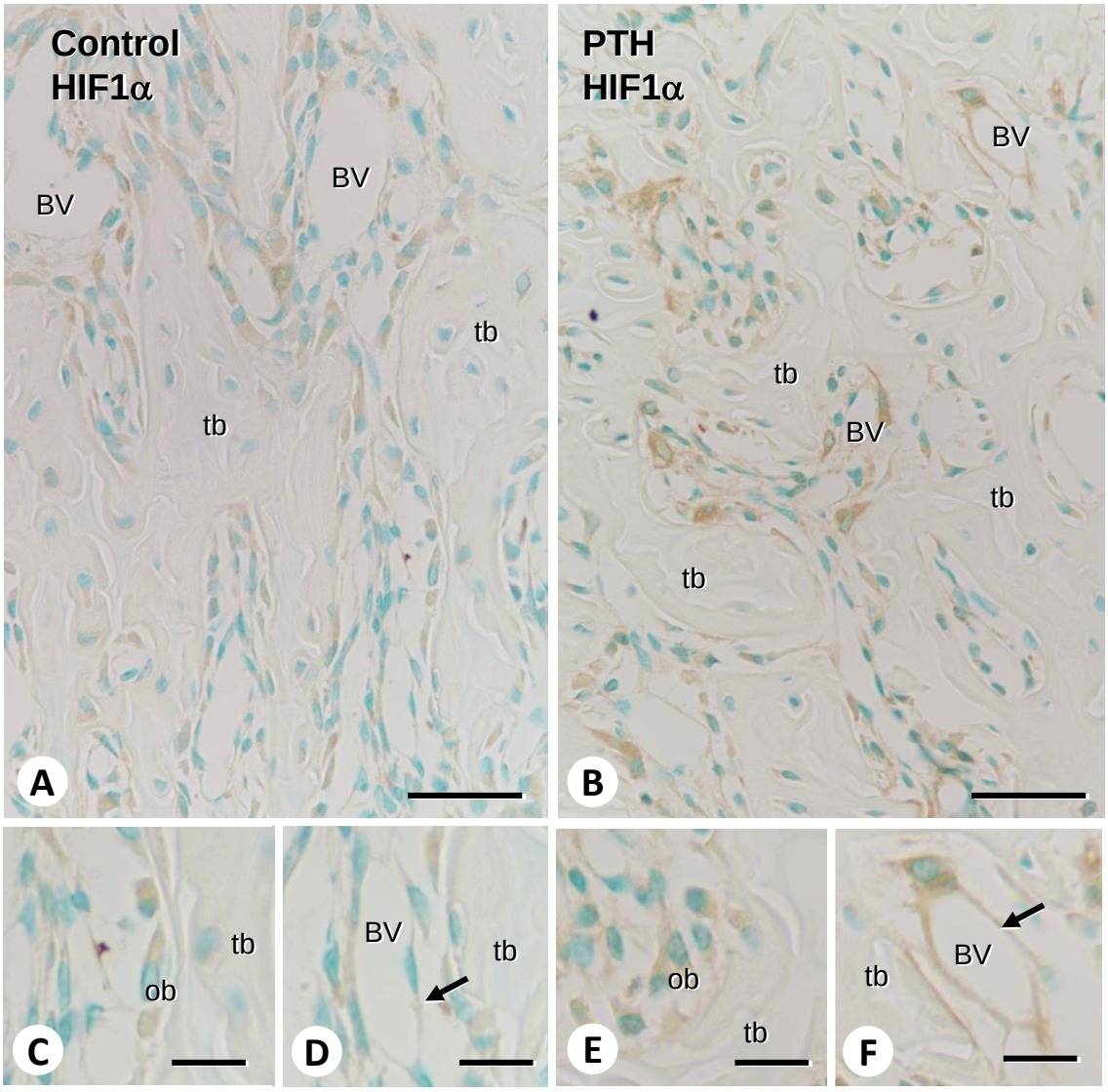
Control
HIF1α
BV
BV
tb
tb
A
PTH
HIF1α
BV
tb
BV
tb
tb
B
tb
ob
C
BV
tb
D
ob
tb
E
BV
tb
F

Fig.3

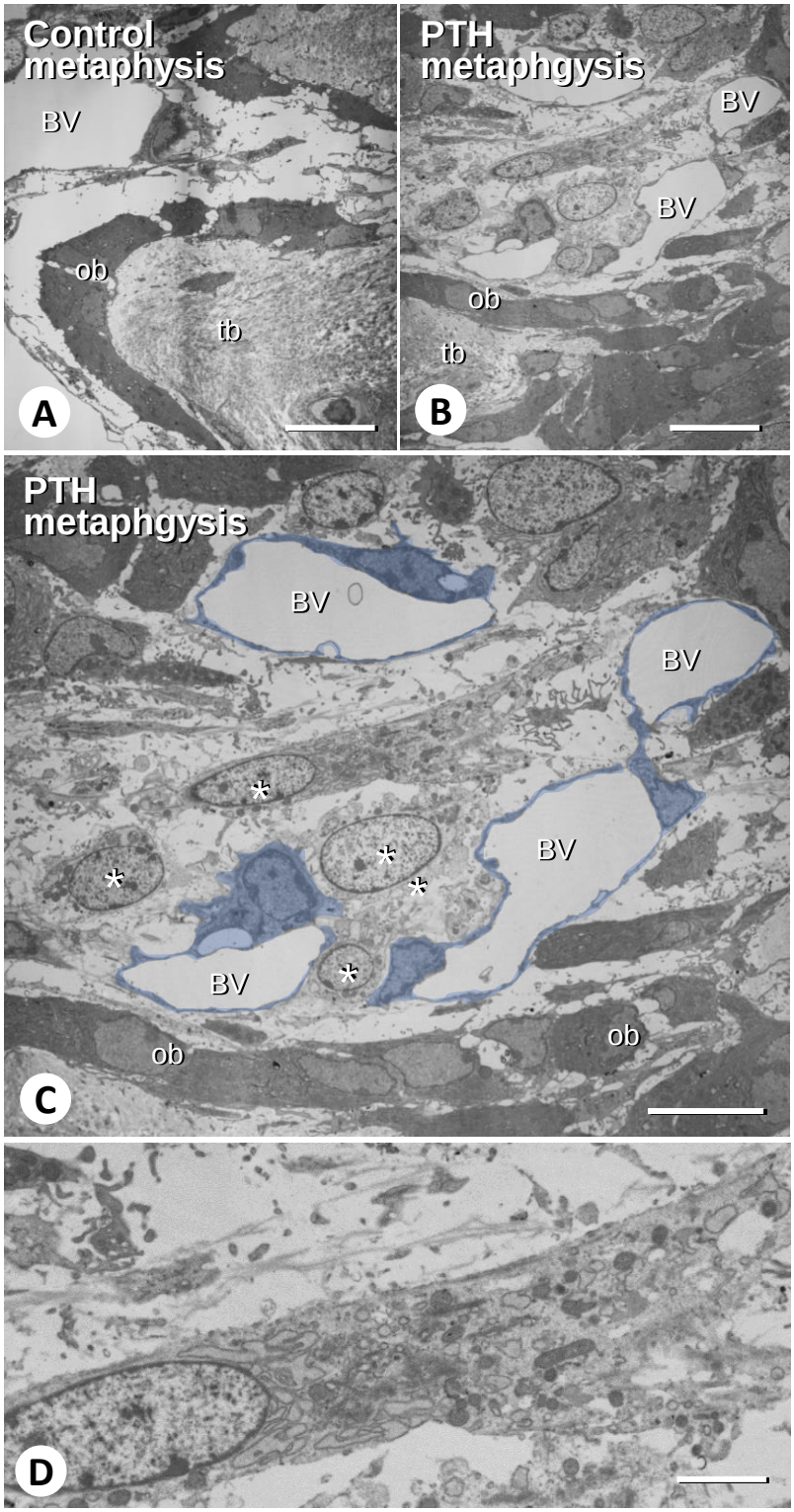
Control
metaphysis
BV
ob
tb
A
PTH
metaphgysis
BV
BV
ob
tb
B
PTH
metaphgysis
BV
BV
BV
BV
ob
ob
C
D

Fig.4

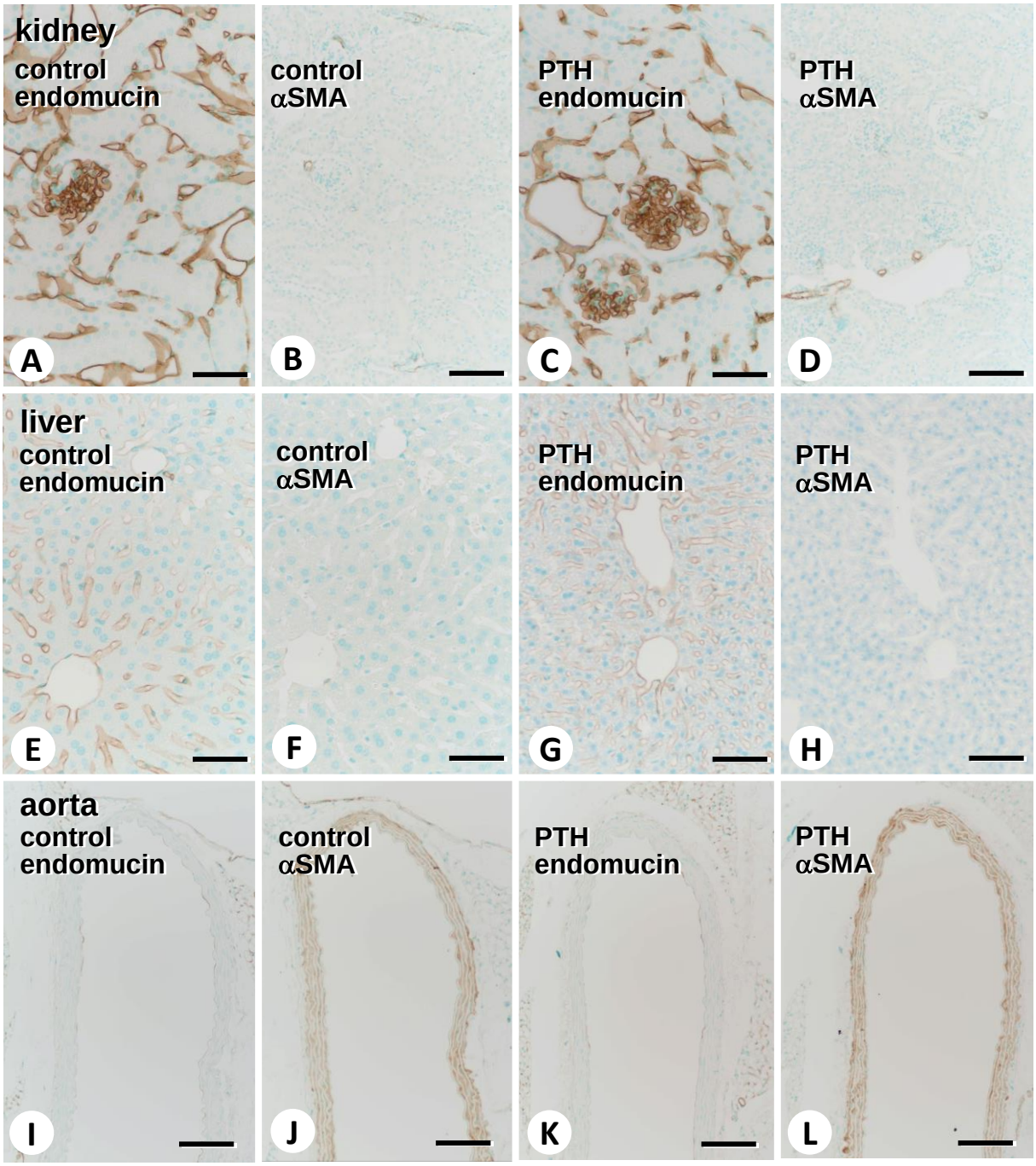
kidney
control
endomucin
A
control
αSMA
B
PTH
endomucin
C
PTH
αSMA
D
liver
control
endomucin
E
control
αSMA
F
PTH
endomucin
G
PTH
αSMA
H
aorta
control
endomucin
I
control
αSMA
J
PTH
endomucin
K
PTH
αSMA
L

Fig.5

Figure legends

Figure 1

Distribution of endomucin-positive blood vessels and αSMA- and ephrinB2-immunoreactive cells after intermittent PTH administration in the femoral metaphysis

Panels **A**-**F** show the double detection of endomucin (red color)/αSMA (green color) (**A, D**), endomucin (red color)/ephrinB2 (green color) (**B, E**), and αSMA (red color)/ephrinB2 (green) (**C, F**) via immunohistochemistry in the control (**A-C**) and PTH-treated (**D-F**) specimens, respectively. αSMA-immunopositive blood vessels and αSMA-reactive cells surrounding the blood vessels are markedly increased after PTH administration (**D**, see the arrows) compared to the control specimens (**A**). In addition, many ephrinB2-reactive cells (arrows) surround the endomucin-positive blood vessels in the PTH-treated mice (see inset in **E**), while endomucin-positive blood vessels in the control mice are located away from ephrinB2-osteoblasts on the bone surface (**B**). The double detection of αSMA and ephrinB2 reveals that ephrinB2-reactive cells co-localize with αSMA around the blood vessels after PTH administration (indicated by white arrows in **F**).

BV: blood vessel, tb: trabecular bone, ob: osteoblasts

Bars, **A, D**: 100 μm, **B, C, E, F**: 50 μm

Figure 2

Immunolocalization of EphB4-immunoreactive cells in bone after PTH administration

Panels **A**, **B** show immunolocalization of EphB4 (brown color) in the femoral metaphyses of control (**A**) and PTH-treated (**B**) mice. The control specimens exhibit EphB4-positive vascular endothelial cells (marked with an arrow in **A**), while PTH-treated specimens reveal not only EphB4-positive vascular endothelial cells but also many EphB4-positive cells around the blood vessels (**B**). Panels **C** and **D** are semi-thin sections of control (**C**) and PTH-treated (**D**) metaphyses stained with toluidine blue. A few preosteoblasts and bone marrow cells are located between the osteoblasts and blood vessels in the control sections (**C**). After PTH administration, many preosteoblasts and interstitial stromal cells (asterisks) are visible in the corresponding area (**D**).

tb: trabecular bone, BV: blood vessel, ob: osteoblast, pob: preosteoblast

Bars, **A, B**: 50 μm, **C, D**: 10 μm

Figure 3

Immunolocalization of HIF1α in the femoral metaphysis after PTH administration

Panels **A-F** show the immunohistochemistry staining of HIF1α (brown color) in control (**A, C, D**) and PTH-treated (**B, E, F**) specimens. Whereas the control specimens display faint HIF1α immunoreactivity on osteoblasts (brown color, **C**) and blood vessels (arrows, **D**), intense immunoreactivity for HIF1α can be seen on osteoblasts (brown color, **E**) and blood vessels (arrows, **F**) after PTH administration.

tb: trabecular bone, BV: blood vessel, ob: osteoblast

Bar, **A, B**: 20 μm, **C-F**: 10 μm

Figure 4

TEM observation of the stromal cells between blood vessels and osteoblasts in the femoral metaphysis after PTH administration

The TEM images show abundant stromal cells (asterisks, **C**) accompanied with blood vessels (blue color, **C**) located on the bone marrow region in the femoral metaphyses of PTH-treated mice (**B**), whereas only a few preosteoblasts with poor cell organelles and cytoplasm can be seen overlying osteoblasts in the control mice (**A**). At higher magnification of PTH-treated specimens, stromal cells display numerous cell organelles, including rough endoplasmic reticulum in their cell bodies (**D**).

tb: trabecular bone, BV: blood vessel, ob: osteoblast

Bar, A-**C**: 10 μm, **D**: 3 μm

Figure 5

Immunohistochemistry of endomucin and αSMA in the kidney, liver, and aorta of control and PTH-treated specimens

The specimens obtained from the kidney in both control and PTH administrated mice demonstrate the immunoreactivity of endomucin on the vascular endothelial cells of glomeruli and peritubular capillaries (brown color, **A, C**); however, they exhibit very little *αSMA*-positivity on the arteries and veins (**B, D**). In the liver, the vascular endothelial cells of central veins and sinusoidal capillaries reveal the immunoreaction of endomucin in both control and PTH-treated mice (brown color, **I, L**), although αSMA-positivity cannot be seen on the corresponding area (**F, H**). The aorta of control and PTH-treated-mice exhibit very faint

endomucin-positivity on the vascular endothelial cells of tunica intimae (**I, K**) and intense αSMA-immunoreactivity on the vascular smooth muscle cells of tunica media (**J, L**),
Bar, **A-H**: 50 μm, **I-L**: 100 μm